Materials & Design 237 (2024) 112578

Contents lists available at ScienceDirect

Materials & Design

journal homepage: www.elsevier.com/locate/matdes

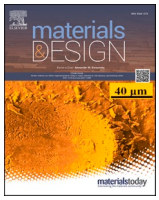

Crosslinking and pyrolysis of a methyl-silsesquioxane: Effect of heating rate on fabrication of polymer derived mullite ceramics using thermoplastic shaping

Fateme Sarraf [a,b,*], Amir Hadian [a,c], Frank Gfeller [b], Sergey V. Churakov [b,d], Frank Clemens [a,*]

[a] Empa-Swiss Federal Laboratories for Materials Science and Technology, Ueberlandstrasse 129, CH-8600 Dübendorf, Switzerland
[b] University of Bern, Hochschulstrasse 6, CH-3012 Bern, Switzerland
[c] Fachhochschule Nordwestschweiz FHNW, Klosterzelgstrasse 2, CH-5210 Windisch, Switzerland
[d] Paul Scherrer Institute, Forschungsstrasse 111, CH-5232 Villigen, Switzerland

ARTICLE INFO

Keywords:
Preceramic polymers
Methyl-silsesquioxane
Polyoctahedral silsesquioxanes (POSS)
Silicate
Fused deposition modeling

ABSTRACT

Poly-silsesquioxanes have been numerously used to produce SiO_2 or $Si_xO_yC_z$ ceramics through pyrolysis under different atmospheres. In this study, crosslinking and pyrolysis behavior of a commercial methyl-silsesquioxane, was examined using thermogravimetry analysis and a lower SiO_2 yield was observed after pyrolysis at low heating rates of 0.3 and 0.6 K/min under air atmosphere, namely 69.1 and 75.0 wt%, respectively. Using ceramic thermoplastic shaping techniques, a low heating rate, below 2 K/min, is usually required to remove processing additive (e.g., binders) gradually and avoid failures like blisters, pores, and cracks. A mixture of SILRES® MK and γ-Al_2O_3 was prepared to produce a mullite ceramic with Al_2O_3/ SiO_2 ratio of 60/40 wt%. As expected, the stoichiometric ratio of alumina to silica was altered using a heating rate of 0.6 K/min and mullite ceramic with 61.70/37.70 wt% of Al_2O_3/ SiO_2 ratio was obtained. By mixing above the crosslinking temperature of SILRES® MK, a constant ratio of alumina to silica could be achieved successfully, even at low heating rates. In addition, microstructure indicated the growth of needle-like mullite crystals with some amount of SiO_2-rich ternary amorphous phase (MgO–Al_2O_3–SiO_2) between the needle grains. Elemental analysis revealed that MgO sintering additive was mainly in the amorphous SiO_2-rich phase.

1. Introduction

Use of molecular precursors to produce ceramic structures was first introduced by the studies of Ainger and Herbert in 1960 [1]. Synthesis of SiC ceramics from polycarbosilane published by Yajima et al. in 1975 initiated a major advance in the field of polymer pyrolysis to produce polymer derived ceramics (PDCs) [2]. Since then, numerous research studies have been conducted on the fabrication of amorphous or nano-crystalline PDCs, particularly ceramics such as SiC [3], Si_3N_4 [4], SiCN [5], SiOC [6,7], SiBCN [8]. While most of the publications focus on the synthesis of non-oxide ceramics using an inert atmosphere (e.g. nitrogen or argon), there are several reports on synthesizing silicate and oxy-nitride ceramics including mullite [9], wollastonite [10], zircon [11], cordierite [12], SiAlONs [13], and more [14] under air atmosphere.

Although a wide variety of materials has been synthesized using preceramic polymers, researchers have mainly focused on the fabrication of coatings [15–17], thin structures [18], foams and porous structures [19–21]. The reason is that the intensive release of gaseous byproducts during crosslinking and pyrolysis and the high shrinkage of these polymers during transformation into ceramics can cause cracks, blisters, or bubbles when larger parts are processed [22]. To avoid crack formation by controlling the shrinkage during pyrolysis, Greil in 1995 introduced addition of non-volatile fillers, including metal and ceramic particles and reduced the shrinkage to a great extent [23]. Another reason for the formation of cracks, blisters and bubbles is the intensive release of gaseous byproducts during thermal crosslinking and pyrolysis in bulk structures (around a few mm^3) [24]. Therefore, a partially water soluble binder system and a low heating rates (e.g. 2 K/min or less) is of great importance to be able to gradually remove the gaseous products during the thermal treatment and avoid such typical structural defects [24,25].

For shaping complex PDC parts, different additive manufacturing

* Corresponding authors at: Empa-Swiss Federal Laboratories for Materials Science and Technology, Ueberlandstrasse 129, CH-8600 Dübendorf, Switzerland.
E-mail addresses: Fateme.sarraf@empa.ch (F. Sarraf), frank.clemens@empa.ch (F. Clemens).

https://doi.org/10.1016/j.matdes.2023.112578
Received 26 September 2023; Received in revised form 30 November 2023; Accepted 12 December 2023
Available online 15 December 2023

(AM) methods including UV-assisted AM, laser assisted and extrusion based AM methods have been used. Processes like stereolithography [26,27], digital light processing (DLP) [28,29], selective laser sintering [30,31], direct ink writing (DIW) [32,33] and material extrusion additive manufacturing (MEX-AM) [18,24,34–38] are AM methods that have been used for PCP materials. Material extrusion additive manufacturing (MEX-AM), previously called fused deposition modeling (FDM), fused filament fabrication (FFF) or fused deposition of ceramics (FDC), has been employed because of thermoplastic properties of some PCP materials. However, because of thermal crosslinking, low processing temperatures are typically used. Mei et al. in 2019 successfully fabricated SiOC honeycomb structures using a commercial methyl-silsesquioxane resin, known as SILRES MK, with zinc acetylacetonate hydrate serving as the crosslinking catalyst under an argon atmosphere [37]. Carbon fibers were incorporated as the reinforcing component, while PLA was utilized as the thermoplastic binder to create a printable filament. The samples were printed at 210 °C, followed by a crosslinking step at 150 °C for 2 h. Amorphous SiOC structures were obtained by heating samples up to 1100 °C under argon atmosphere. Gorjan et al. in 2019 combined SILRES MK resin and an ethylene vinyl acetate polymer to achieve the plasticity needed for the MEX-AM process [18]. Adding an alumina source with a stoichiometric ratio of 3:2 between Al_2O_3 and SiO_2, a 3:2 mullite phase was reached after sintering at 1550 °C in air. Hollow struts made of SiOC were produced by Kulkarni et al. in 2020 through the pyrolysis of impregnated 3D-printed PLA structures with a liquid polysiloxane [36]. Three-dimensional β-SiC ceramics were fabricated by Zhao et al. in 2021 using a polycarbosilane precursor [34]. To achieve sufficient thermoplastic behavior for printing, a polypropylene binder was utilized. After printing the feedstock below 300 °C, samples went through an oxidative crosslinking at 200 °C, using a heating rate of 2 K/min. Subsequently, the samples were pyrolyzed for 2 h at 1200 °C under an argon atmosphere. XRD analysis of the final structures exhibited the formation of β-SiC ceramics with an amorphous SiO_xC_y content. Furthermore, Chawich et al. in 2022 conducted a study where SiCN and SiC cellular ceramic structures were produced using PolyVinylSilazane (PVZ) and AllylHydridoPolyCarboSilane (AHPCS) in combination with DiCumyl Peroxide (DCP) as a crosslinking agent [35]. Initially, PLA molds were created using a filament printer. Subsequently, these printed molds were subjected to a dip coating process, where they were coated six times with mixtures of PVZ/DCP or AHPCS/DCP. The impregnated molds were then pyrolyzed at 1000 °C for 2 h, with a heating rate of 2 K/min under nitrogen and argon atmosphere to obtain amorphous SiCN and SiC ceramics, respectively.

As mentioned earlier, a low heating rate for MEX-AM is required to avoid structural defects like cracks, blisters and bubbles. Tian et al. in 2012 demonstrated that pore size and porosity of polymer derived foams can be tailored by changing the heating rate below crosslinking temperature, which indicates that the residue of PCP materials is affected by the heating rate [39]. To obtain SiOC foams, different heating rates (0.25–3 K/min) were used to crosslink the silicone resin up to 250 °C in air. Consequently, pyrolysis and sintering was performed at 1200 °C, with a heating rate of 5 K/min in Ar atmosphere. It could be demonstrated that spherical pores in form of an open-cell were formed when using a heating rate below 1 K/min. Maximum open porosity of 72.5 vol % was obtained at a heating rate of 0.5 K/min.

Although synthesis and fabrication of various PDC powders and parts have been investigated under different atmospheres using various thermal programs, there is no literature on comparing the pyrolysis behavior under air and inert atmospheres and the effect of the heating rate on ceramic yield after pyrolysis to the best of our knowledge. However, this aspect is of significant importance as precise stoichiometric ratios for the synthesis of polymer derived silicate ceramics, are crucial based on the studies by Bernardo et al. in 2006 [40] and Gorjan et al. in 2019 [18]. Therefore, in this study, we investigated the effect of thermal treatment conditions on the ceramic yield of a commercial methyl-silsesquioxane preceramic polymer under three different atmospheres (air, nitrogen and argon) up to 800 °C and studied the crucial effect of heating rate on crosslinking and pyrolysis of MK under oxidative atmosphere in more details. Subsequently, the effect of the SiO_2 yield on the stoichiometric composition of mullite (the Al_2O_3:SiO_2 ratio and the formed mullite phase) was investigated using extruded filaments, containing thermoplastic binder composition. Such filaments have the potential to be used for ceramic thermoplastic shaping methods like pressing, extrusion, injection molding and MEX-AM [41,42]. In this way, fabricating a wide range of polymer derived silicates with precise compositions and diverse geometries will be feasible.

2. Material and methods

2.1. Materials

A commercial polysilsesquioxane resin powder, SILRES® MK (abbreviated MK, Wacker–Chemie GmbH, Germany), containing methyl groups, was used. According to the manufacturer, approximately 82 wt % SiO_2 content after pyrolysis at 1000 °C in air was expected. MK contains functional OH groups that enables it to undergo thermal crosslinking via polycondensation reactions [43,44].

In order to achieve a SiO_2-rich mullite phase, 40 vol% of powder consisting of 29.95 wt% of alumina powder (γ-Al_2O_3-PURALOX SCFa-140 UF3, Sasol Performance Chemicals Ltd) and 24.34 wt% of MK were mixed with 60 vol% of thermoplastic binder. The thermoplastic binder contained 25.95 wt% polyvinyl alcohol (PVA, Sigma-Aldrich) and 19.24 wt% ethylene vinyl acetate copolymers (Elvax 460, DuPont, International SARL). To improve the sinterability of the mullite phase, 0.52 wt% of magnesium oxide (MgO, Fluka™) was added to the mixture. The mixture composition is described in more detail elsewhere [24]. Initially, the binder components were melted in the chamber of a torque rheometer equipped with roller-rotors mixing elements (Rheomix 600, HAAKE™ PolyLab™ OS, Thermo Fisher Scientific, Germany). Then, dry powders were gradually added to the mixing chamber. MK starts thermal crosslinking at temperatures above 160 °C [45]; therefore, batches (feedstocks) were mixed below and above the thermal crosslinking temperature of the MK, namely 160 and 190 °C. The two feedstocks were extruded at 150 and 160 °C, respectively, in the form of rods with a capillary rheometer (Rosand RH10, NETZSCH-Gerätebau GmbH, Germany). Binder removal occurred in two steps including solvent and thermal debinding; First PVA was removed by immersing the rods in a water bath [24] followed by wick debinding of the remained binder at 210 °C for 48 h in a box furnace (Pyrotec PC 12, Michel Keramikbedarf, Switzerland). Then, rods were heated up to 800 °C to remove all the binder and paralyze MK with two different heating rates (0.6 and 20 K/min). Finally, sintering was carried out at 1700 °C for 5 h in a furnace equipped with $MoSi_2$ heating elements (LHT 03/17 D, Nabertherm GmbH) to ensure the full transformation to mullite.

2.2. Characterization

To investigate the effect of the heating rate and the atmosphere on the yield of SiO_2, MK was heated to 800 °C in different atmospheres. Thermal analysis of MK was performed using a constant amount of powder heat-treated under air, argon (Ar) and nitrogen (N_2) atmosphere by DTA/TGA instrument (STA 449 F3 Jupiter, Netzsch GmbH, Germany) with a constant gas flow of 70 ml/min and different heating rates, namely 0.3, 0.6, 2, 5, 10 and 20 K/min.

To characterize the exhaust gases from the pyrolysis of MK, a transfer line at 250 °C was used to carry the pyrolysis products of MK heated to 800 °C with a rate of 20 K/min to a combined gas chromatograph and mass spectrometer (GC 7890B-MS5977 B, Agilent, USA), called GC–MS instrument. Two configurations were used for these studies. First, gaseous species were collected in 20 °C intervals and frozen in a cryogenic trap at temperature of −150 °C before the inlet of the GC column. At the end of the TG analysis, the cryogenic trap was heated and the

GC–MS analysis was performed. The gaseous species were separated by a fused silica capillary column (HP 5 ms UI, Agilent, USA) coated with (5 %-phenyl)-methylpolysiloxane stationary phase under a programming temperature condition; 35 °C (2 min hold) – (10 K/ min) – 300 °C (20 min hold). Gas species with $33 < M_w < 550$ were identified with the MS unit. In the second configuration, the pyrolysis products were transferred directly to the MS using a bypass line to investigate the actual temperature of released gaseous species. The NIST mass spectral search program was used to analyze the data.

To investigate the MK bond characteristics as received, after crosslinking and pyrolysis, Fourier-transformed infrared spectroscopy (FT-IR) spectroscopy measurements were performed at room temperature with Tensor 27 (Bruker, Germany) equipped with a diamond attenuated total reflectance (ATR). Optical transmission data were collected from 600 to 1800 cm^{-1} with a resolution of 4 cm^{-1} and with 32 scans.

To verify the thermal crosslinking behavior of SILRES® MK, a rotational rheometer (MCR 302, Anton Paar, Austria) was used. Measurements were performed with a plate-plate system at a constant shear rate of 1 s^{-1}.

X-ray diffraction (XRD) analysis of sintered samples were performed using a X-ray diffractometer (EMPYREAN, Malvern PANalytical Ltd., UK) equipped with a Cu X-ray source (45 kV/40 mA) and a 1 Der detector. Fixed divergence slit of 0.25° and 0.02° radian soller slits were used. Measurements were carried out between 2Θ of 5-90° with a step size of 0.0167°/step at 120 s/step.

Using X-Ray Fluorescence (XRF), chemical mass analysis of mullite powders was obtained to quantify each oxide content. Fused beads were prepared from a 1:10 sample:flux mixture. The flux used was "Claisse Borate Flux" from Malvern PANalytical with 66.67 % $Li_2B_4O_7$, 32.87 % $LiBO_2$ and 0.5 % LiI. The wavelength dispersive XRF spectrometer (Zetium, PANalytical Ltd., Netherlands) was used for bulk chemical analysis. The instrument calibration is based on the PANalytical WROXI software. The XRF analytical procedure employing WROXI software was established using sets of PANanalytical materials based on 200 international Certified Reference Materials (CRM's).

The microstructure of sintered mullite structures was investigated by scanning electron microscopy (ESEM Quanta FEG 650, FEI, USA). To detect the elemental composition of crystalline and amorphous phase, sintered samples were sputtered with carbon after polishing the embedded samples in resin and were studied using energy dispersive X-ray spectroscopy (EDS) analysis (UltraDry Silicon Drift Detector (SDD), Thermo Fisher Scientific Inc., USA) with a detector size of 60 square millimeters.

3. Results and discussion

3.1. Thermogravimetry analysis of MK

At the beginning of this study, we investigated the ceramic yield of the MK preceramic polymer by simultaneous thermal analysis (STA) using different heating rates and atmospheres. As can be seen in Fig. 1, MK yielded the same amount of ceramic after heating up to 800 °C using different heating rates under nitrogen and argon atmosphere. A constant yield of 82 wt% was obtained which confirms the reported yield by the manufacturer. The observations are in good agreement with the reported values by Ma et al., where they studied the pyrolysis of VTES (vinyltriethoxysilane)/ TEOS (tetraethoxysilane) system with different heating rates under argon atmosphere to achieve SiOC aerogels, obtaining a stable SiOC yield [46].

Pyrolysis under air atmosphere, however, resulted in an unexpectedly higher mass loss when a heating rate below 2 K/min was used. A SiO_2 residue of 69.1 wt% and 75.0 wt% was achieved using 0.3 and 0.6 K/min heating rates, respectively. The occurrence of such low yield means that the lower the heating rate, the higher the chance to evaporate unlinked low molecular weight symmetric species before any crosslinking (polycondensation reactions) occurs. Tian et al. [39] observed an effect of heating rate up to crosslinking temperature (250 °C) in air atmosphere and were able to fabricate preceramic foams with different pore sizes and porosity. Although they did not investigate the change of mass loss with heating rate, it was shown that by decreasing the heating rate from 3 K/min to 0.5 K/min, higher porosity and higher pore sizes were achieved due to the higher release of volatiles.

To make silicate ceramics by PCP route, typically debinding and sintering in air is used; therefore, a non-stoichiometric composition of the silicate ceramic can be expected using low heating rates or dwell times at critical temperatures during the thermal debinding, typically used in MEX-AM process.

To explore this phenomenon further, additional investigations were conducted into the pyrolysis of MK in air atmosphere. As shown in Fig. 2,

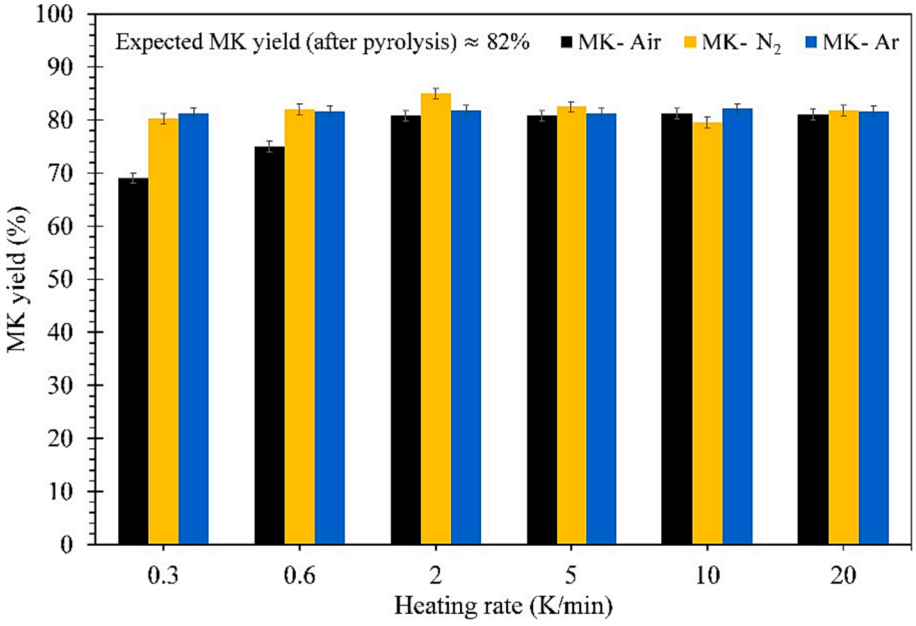

Fig. 1. Yield of MK preceramic polymer heated to 800 °C with heating rates, between 0.3 and 20 K/min, under three different atmospheres (air, N_2, Ar).

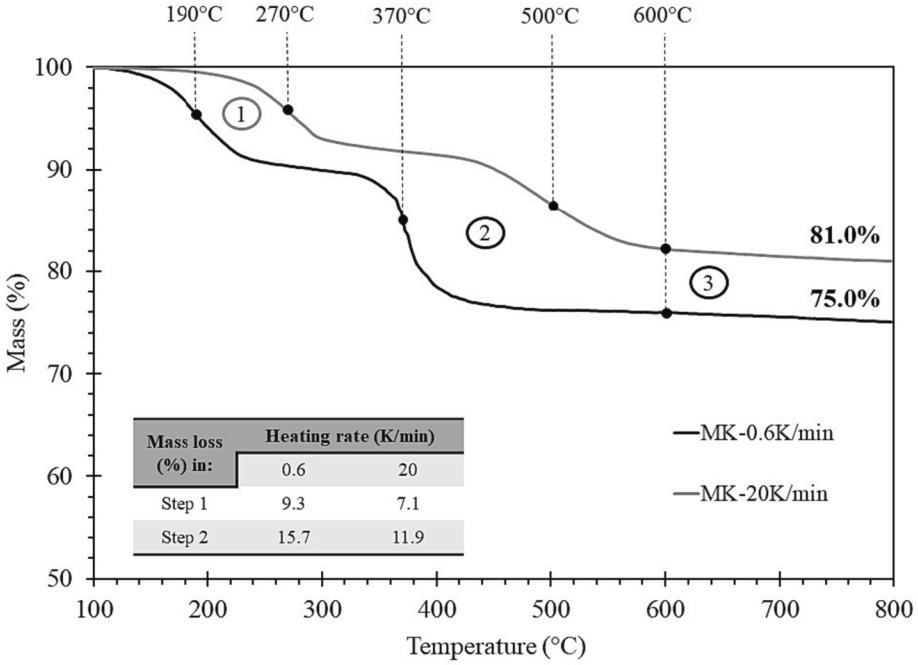

Fig. 2. TG analysis of MK heated up to 800 °C with a heating rate of 0.6 and 20 K/min under air.

the thermal evolution of MK occurs in two steps corresponding to its crosslinking (polycondensation reactions) and pyrolysis (ceramization). For comparison, only two heating rates, namely 0.6 and 20 K/min, were chosen to demonstrate the dependence of the SiO_2 yield on the heating rate after heat treatment up to 800 °C. Crosslinking with 0.6 K/min occurred at a temperature range between 100 and 250 °C, whereas for a heating rate of 20 K/min, the crosslinking continued up to higher temperatures (100 °C to 305 °C). A second mass loss appeared in the range of 310–440 °C and 400–590 °C for the heating rate of 0.6 K/min and 20 K/min, respectively. In steps 1 and 2, the MK sample heat treated with a rate of 0.6 K/min, released 2.2 and 3.8 % more volatiles in comparison to the heat treatment with 20 K/min, respectively.

3.2. GC–MS analysis of MK up to 800 °C

To investigate the gaseous species released during the crosslinking and pyrolysis steps and determine the underlying causes for the unstable SiO_2 yield during PCP processing in air atmosphere, gas chromatography/mass spectrometry (GC–MS) equipment was used. The MK was heated up to 800 °C and the gases were collected between 100 °C and 800 °C. Cryo-trap setup was used to collect the gas species during thermal treatment. As shown in GC–MS analysis in Fig. 3a, two sets of peaks could be detected at low (i.e. 1–5 min) and high (i.e. 12–20 min) retention times. The peaks appearing at lower retention times belonged to low molecular weight gas species with higher polarity. Due to the application of a non-polar stationary phase in GC, these high polarity species were released earlier. In Table 1, the identified gas molecules associated with lower retention times included mainly carbon dioxide (CO_2), acetaldehyde (C_2H_4O), ethanol (C_2H_6O) and acetone (C_3H_6O). The peaks appeared at high retention times corresponded to the POSS (Polyhedral Oligomeric Silsesquioxane) molecules with a general chemical formula of $(RSiO_{1.5})_n$ (where n = 4, 6, 8, 10, and 12, and in most cases 8) [47]. Our setup was unable to detect species with molecular weights below 32 (to avoid oxygen background in the chromatogram); therefore, the release of other species such as hydrogen, methane, and water that is mentioned in the literature [45,48], could not be identified in our experiments.

In addition to the GC–MS analysis using a cryo-trap, a bypass was used to detect the temperature ranges at which selected gas species are evolving. Specific *m/z* values of 15, 18, 31, 44 and 521 corresponding to methane, water, ethanol, carbon dioxide and octamethyl-T8 ($C_8H_{24}O_{12}Si_8$, a POSS molecule with Mw = 536) were selected to monitor the crosslinking and the conversion step to amorphous SiO_2 ceramic with a heating rate of 20 K/min up to 600 °C (Fig. 3b). Based on Fig. 3b, release of methane, water, ethanol, carbon dioxide and POSS was observed during the first step of mass loss up to 300 °C. In the second step, the removal of mainly water and carbon dioxide were continued.

According to Lonescu et al., crosslinking due to polycondensation reactions occurred between 170 and 370 °C under an argon atmosphere [48]. In our experiments, however, this step finished earlier as we used air instead of argon atmosphere, which can be explained by additional thermal oxidation processes. Moreover, the release of POSS molecules was reported in both steps. On the contrary, based on our findings, it is apparent that the evaporation of low molecular POSS primarily occurs during the crosslinking process when exposed to air atmosphere. Looking at the mass loss in Fig. 2, we can conclude that if the time of the second step increases due to a lower heating rate, volatile species have more time to disappear and this will result in a higher mass loss.

A schematic chemical structure of MK resin including Si-O-Si cages along with hydroxyl (–OH), methoxy ($–CH_3O$) and $SiCH_3O$ groups is presented in Fig. 4a. As highlighted in this figure, water, ethanol and POSS molecules can potentially be released from the chemical structure. The $SiCH_3O$ groups are responsible for the SiO_2 yield of MK after pyrolysis in air. The POSS molecules containing Si-O-Si bonds can be present in the unstable form of cages or crosslinked dense networks as shown in Fig. 4b. By heating MK, these bonds split, the cages collapse, and dense Si–O–Si network structures start to appear [49]. Based on our results, we assume that using a lower heating rate, the volatile Si-O-Si cage structures have more time to evaporate before crosslinking is completed which will result in a higher mass loss.

3.3. FT-IR of selected MK samples

Based on the GC–MS analysis of pure MK up to 800 °C in air atmosphere, the release of POSS molecules was detected. In order to understand the transition from volatile POSS with Si-O-Si cage structures to a stable Si-O-Si network, which determines the SiO_2 yield after pyrolysis,

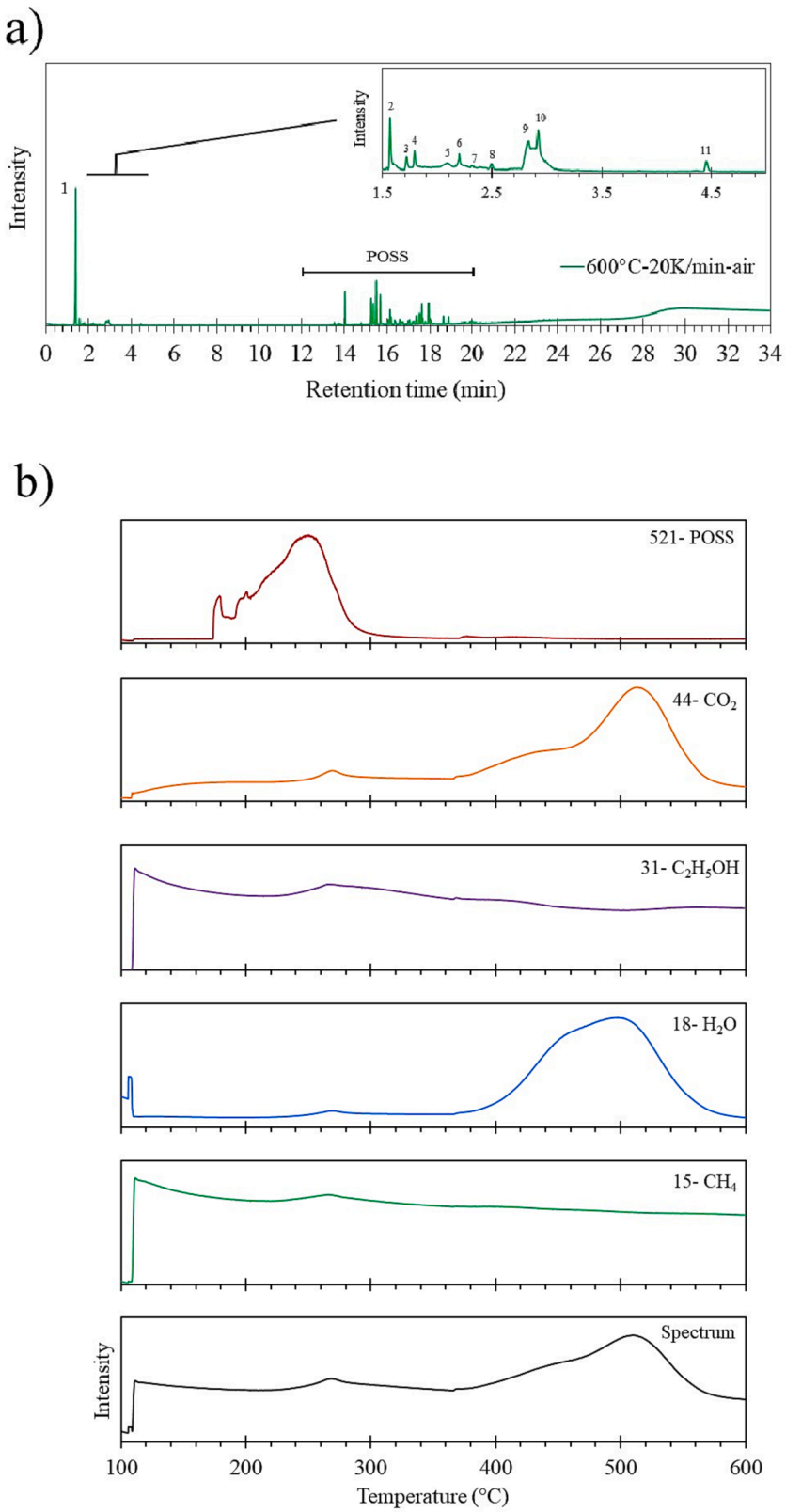

Fig. 3. a) GC–MS chromatograms from MK heated with a rate of 20 K/min up to 800 °C, b) bypass measurement of MK up to 600 °C with a heating rate of 20 K/min for specific *m/z* gas molecules.

the characteristic bonds of MK were analyzed by FT-IR at different stages of heat treatment, using heating rates of 0.6 and 20 K/min. To investigate the right temperatures for this study, DTG plots from TG analyses in Fig. 2 were utilized, and the temperature corresponding to the DTG peak at each step of mass evolution was selected for both heating rates (0.6 and 20 K/min). Two DTG peaks are expected for each heating rate which indicates the maximum mass loss rate during crosslinking and pyrolysis steps. For further investigations, 190 and 270 °C, as representatives of

Table 1
Identified peaks with retention time between 1 and 5 min.

Peak No.	1	2	3,5	4	6,7	8	9	10	11
Compound	CO_2	C_2H_4O	C_2H_6O	C_3H_6O	$C_6H_8N_2O_8$	–	$C_4H_{10}O_3$	C_6H_6	C_7H_8
Mw	44	44	46	58	236	-	106	78	92

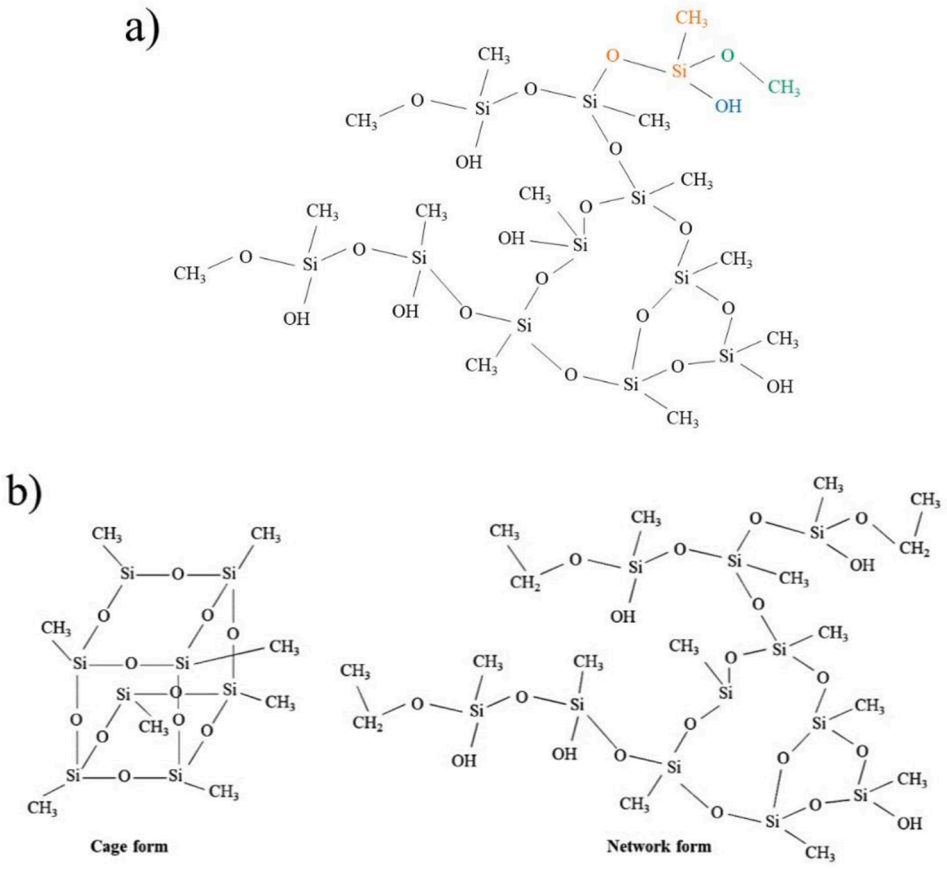

Fig. 4. a) the schematic molecular structure of mk resin indicating different species removed by heating up to 800 °C, b) Methyl-silsesquioxane (abbreviated MSQ, R = CH_3) in form of the cage (T8 structure) and network (based on [50]).

mass loss- step 1, and 370 and 500 °C, as representatives of the mass loss-step 2, were chosen for heating rates of 0.6 and 20 K/min, respectively. Also, a sample at 600 °C was analyzed for both heating rates after pyrolysis. Selected samples are presented in Table 2.

FT-IR analysis of raw MK can be seen in Fig. 5a. Si–CH_3, O-Si-CH_3, Si–O–C, δ-CH_3 and Si–O–Si transmission bands were identified as characteristic signals of polymethylsilsesquioxes in the polymeric state [45,51]. A combination of Si-O-Si bonds in the form of cages (ν_{cage} = 1095 cm^{-1}) and network (ν_{net} = 1010, 1060 cm^{-1}) existed in raw MK before crosslinking step [49,52]. Samples T190H0.6 and T270H20 were used to investigate the atomic bonds after crosslinking and same transmission bands were observed for both samples as in raw MK (Fig. 5a). Raising the temperature to 370 and 500 °C with heating rates of 0.6 and 20 K/min respectively, noticeable changes in the transmission bands of T370H0.6 and T500H20 were detected (Fig. 5b). As can be seen in regions I and II, Si–CH_3 bonds still existed in sample T370H0.6; furthermore, a second peak around 795 cm^{-1} attributed to two different bonds, namely Si-C and Si-O-Si [53,54]. In comparison, for sample T500H20 only the peak at 795 cm^{-1} was observed. Additionally, there was no evidence of Si–CH_3 bonds after pyrolysis (T = 600 °C) regardless of heating rate and only the peak at 795 cm^{-1} persisted. Also, C = O bond, already formed at 370 and 500 °C, was present in both samples. After the pyrolysis, broad peaks in the range of 960–1125 cm^{-1}, interestingly shifted in different directions. In sample T600H0.6, Si-O-Si

Table 2
Selected samples for FT-IR analysis.

	Beforeheat treatment	Mass loss- step 1		Mass loss- step 2		After pyrolysis at 600 °C	
Sample code(TXHY)	Raw MK	T190H0.6	T270H20	T370H0.6	T500H20	T600H0.6	T600H20
Temperature(T)- [°C]	–	190	270	370	500	600	600
Heating rate (H)-[K/min]	–	0.6	20	0.6	20	0.6	20
Mass loss(%)	–	4.6	4.3	14.5	13.4	24.1	17.8

X is the temperature corresponding to DTG peak at each step of mass evolution in TG plot in °C.
Y is the heating rate for the thermal debinding in K/min.

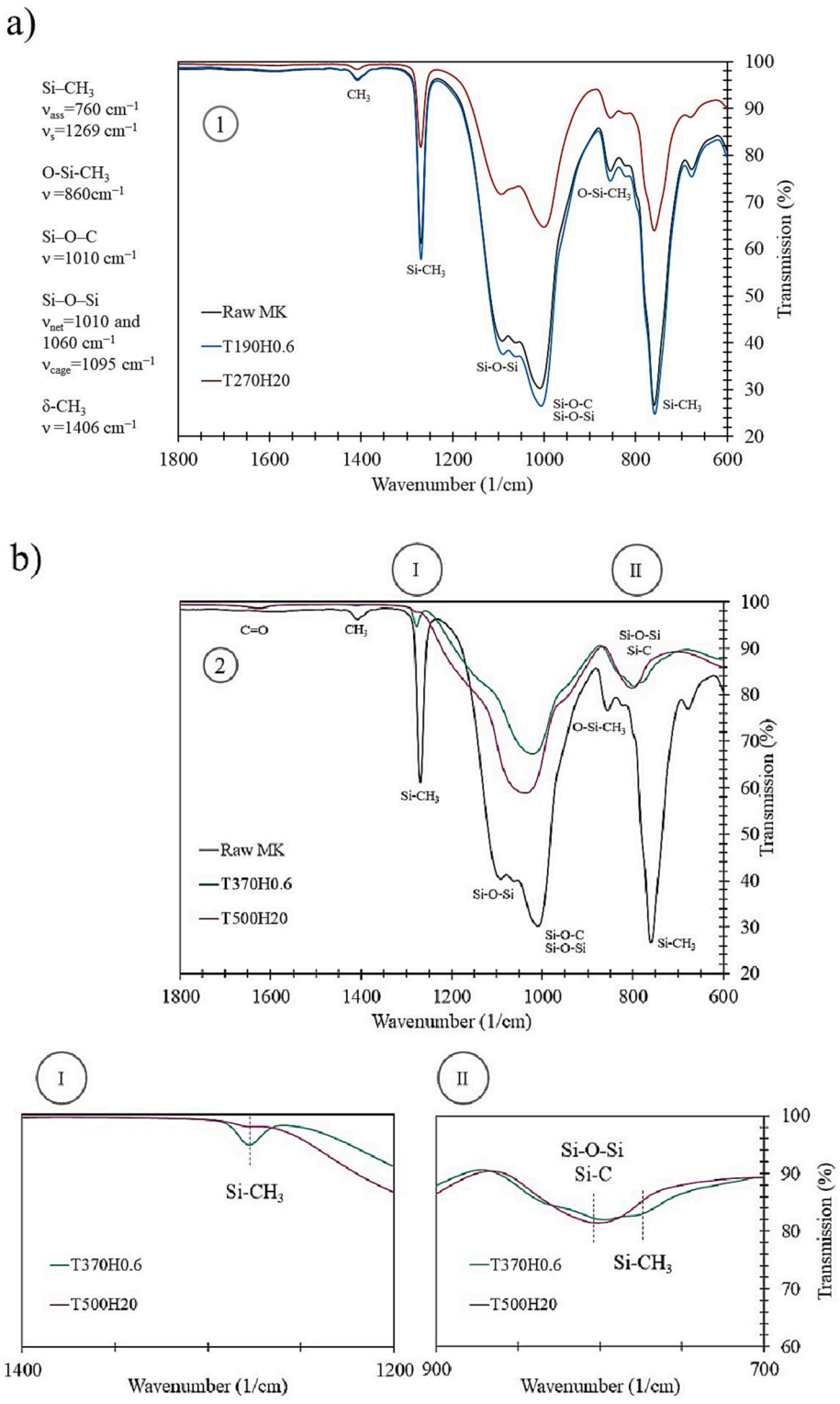

Fig. 5. FT-IR analysis of raw MK compared with a sample after heat treatment at a) 190 and 270 °C, b) 370 and 500 °C, and c) 600 °C with a heating rate of 0.6 and 20 K/min, respectively.

bond in the form of cages seemed to be more prevalent. However, Si-O-C network bond appeared as the dominant feature in sample T600H20.

As shown in Fig. 5a, a combination of Si-O-Si bonds in the form of cages and networks existed in raw MK. In addition, detected Si-CH_3 bonds in FT-IR analysis of raw MK indicated the presence of unstable low molecular POSS species in the form of cages inside the polymer [52]. Both Si-O-Si bond types could still be detected in samples T190H0.6 and T270H20 which showed transformation to a dense Si-O-Si network was not yet completed after crosslinking. Looking at sample T500H20 in Fig. 5b, a significant amount of Si-O-Si network was already formed at 500 °C as Si-SH_3 bonds disappeared. In contrast, due to the remaining Si-CH_3 bonds in sample T370H0.6, we assume that evaporation of POSS

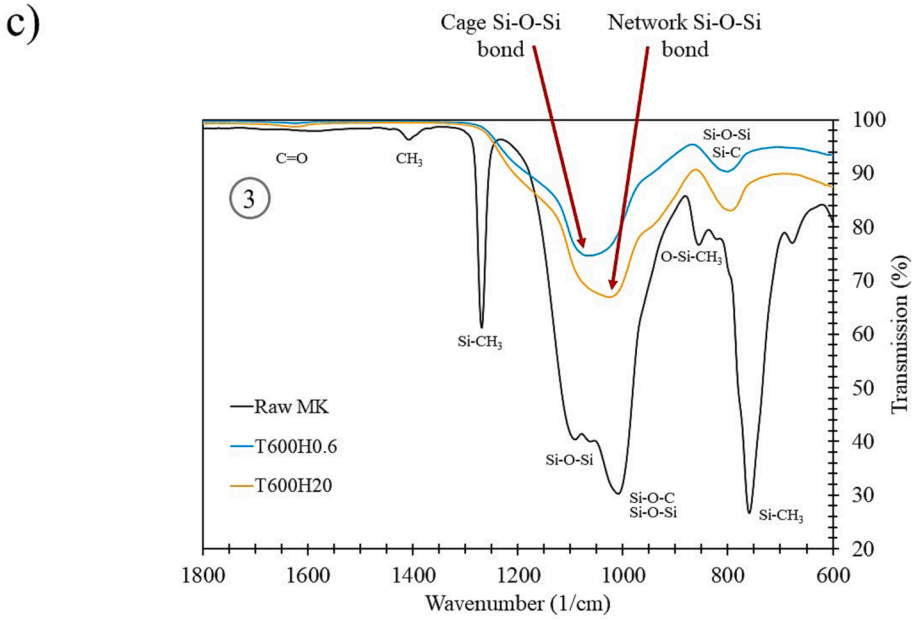

Fig. 5. (*continued*).

species continues up to 600 °C using heating rate of 0.6 K/min. The wide peak around 785–810 cm^{-1} that appeared in both samples is linked to the combined effect of the Si-C and Si-O vibrations bonds formed during the pyrolysis step. The CH_3 bond, which corresponds to the outgassing of ethanol, vanished in both samples T370H0.6 and T500H20 which means no more release of ethanol is expected. C = O bond was formed at 1622 cm^{-1} in both samples indicating the release of carbon dioxide. This finding is in good agreement with the GC–MS bypass analysis (Fig. 3b). Based on the observations in Fig. 5c, we conclude that POSS species in cage form are partially released during the crosslinking step and the remained fraction is stabilized as network Si-O-Si bonds using a heating rate of 20 K/min.

By the FT-IR results, it can be assumed that heating with a rate of 0.6 K/min in air atmosphere resulted in an excessive release of cage POSS species happens during the crosslinking as volatile unstable molecules have more chance to evaporate before stabilizing as network structure, which is consistent with a lower yield for MK-0.6 K/min in Fig. 2.

3.4. Processing of polymer derived mullite ceramics

The results obtained from GC–MS and FT-IR analysis on MK resin show that when the material is subjected to a low heating rate of 0.6 K/min in air, the structure of the resin retains volatile Si-O-Si bonds, leading to a lower amount of SiO_2.

To prove the effect of this phenomenon on the processing of polymer derived mullite ceramic using thermoplastic shaping methods, a SiO_2-rich mullite ceramic was investigated. Therefore, extruded filaments which are suitable for subsequent use in material extrusion additive manufacturing (MEX-AM) methods were studied, because a slow debinding process is needed to remove organic binder (e.g. thermoplastics) during their thermal treatment. Typically, low heating rates (below 1 K/min) and appropriate dwell times are common to ensure the stability of printed structures up to the sintering step. Fig. S1 (appendices) provides an example of a debinding program for MEX-AM of PDCs. Consequently, the fabrication of silicate ceramics that require precise stoichiometric ratios can be challenging.

In order to determine the effect of the heating rate on SiO_2-rich mullite ceramic, a composition of 40 wt% SiO_2 and 60 wt% Al_2O_3 was investigated. Mullite feedstocks were mixed at two different temperatures, namely 160 °C and 190 °C. Torque data over time were recorded for both feedstocks (Fig. 6a,b). By mixing at 160 °C, the torque slightly increased and a torque of ~ 13Nm was achieved after 50 min (Fig. 6a). At a mixing temperature of 190 °C, the behavior of the sample was distinct. Initially, the torque steadily rose to approximately 16 Nm within 60 min. Subsequently, the torque gradually diminished and stabilized around 14 Nm after 80 min (Fig. 6b).

It was assumed that the increase in torque was caused by the thermal crosslinking of MK; therefore, the viscosity of MK resin was measured under constant shear rate of 1 1/s by parallel plate configuration at 160 and 190 °C (Fig. 6c). MK showed a stable viscosity at 160 °C over 20 min. Viscosity at 190 °C, however, started increasing already after 5 min. These measurements confirm the findings of Harshe et al., who observed a similar absence of crosslinking up to 160 °C without using a crosslinking agent [45]. However, when the temperature was increased to 190 °C, thermal crosslinking of the MK resin could be observed (Fig. 6b and c). Based on the last part of the torque analysis during the mixing process, it can be assumed that the crosslinked pieces inside the feedstock were disrupted due to the shear forces applied in the mixing chamber which resulted in a decrease and final plateau in the mixing torque.

3.5. Compositional and microstructural analysis of sintered mullite ceramics

After mixing the composition of 60/40 wt% Al_2O_3/ SiO_2 with thermoplastic binder at two different temperatures, filaments were extruded, debound and sintered at 1700 °C for 5 h. Based on TG results, an Al_2O_3/SiO_2 ratio of 1.52 was expected with a rate of 20 K/min. For the lower heating rate (0.6 K/min), a ratio of 1.64 was expected according to Fig. 2.

As shown in Fig. 6, it is possible to thermally crosslink MK during the mixing process. To investigate this effect, five different samples were investigated (Table 3). Four samples were mixed at 160 °C and 190 °C and pyrolyzed up to 800 °C with a heating rate of 0.6 K/min, among which two were wick debound at 210 °C before pyrolysis as reported elsewhere [24]. In addition, a sample mixed at 190 °C and pyrolyzed up to 800 °C with a heating rate 20 K/min was analyzed, serving as a reference for comparison.

The elemental composition of Al_2O_3, SiO_2 and MgO was investigated using XRF analysis. The calculated Al_2O_3, SiO_2 and MgO contents for

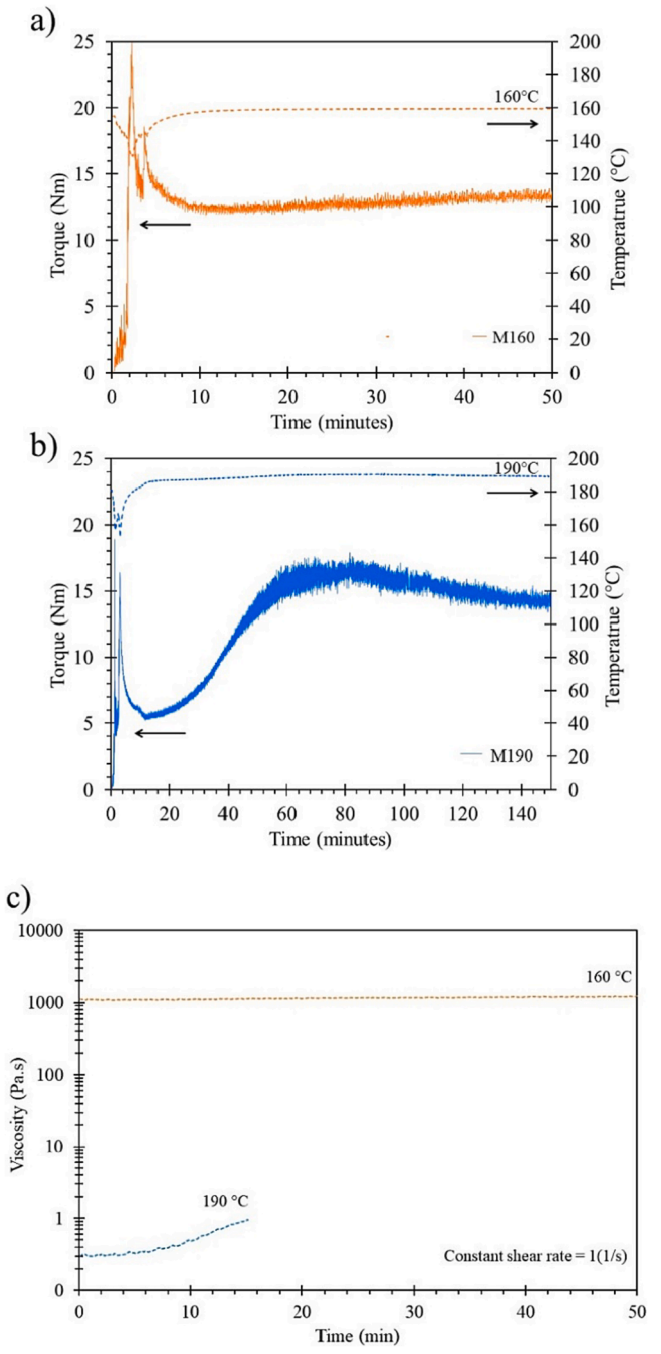

Fig. 6. a,b) torque versus time plot for sample mixed at 160 and 190 °C, labeled as M160 and M190, respectively, c) viscosity versus time plot for pure MK powder at a constant shear rate of 1(1/s).

each sample are presented in Table 3. Notably, the samples mixed at 190 °C consistently exhibited an Al_2O_3/SiO_2 ratio of 1.50, regardless of the heating rate employed during pyrolysis and the implementation of a wick debinding step. On the other hand, the samples mixed at 160 °C displayed a higher Al_2O_3/SiO_2 ratio, ranging from 1.62 to 1.64. XRF result of the sample mixed at 190 °C and heat treated with a rate of 20 K/min aligns well with the findings obtained from TG and FT-IR analyses (Fig. 2 and Fig. 5). By using the fast heating rate, a mass loss of 81 wt% can be confirmed which will result in the expected Al_2O_3/SiO_2 ratio of 1.5. On the other hand, the samples mixed at 190 °C and 160 °C with a heating rate of 0.6 K/min exhibited a completely different behavior. When mixed at 190 °C, the MK starts to undergo crosslinking. This leads to a higher fraction of stabilized POSS molecules that transform into Si-

Table 3
XRF analysis of prepared mullite feedstocks after sintering at 1700 °C for 5 h.

SampleMXX*HYY**	Al_2O_3 (wt%) (2σ= ±0.2)	SiO_2(wt %) (2σ= ±0.15)	MgO (wt %)(2σ= ±0.05)	Al_2O_3/SiO_2	Sum
M160H0.6	61.70	37.70	0.51	1.64	99.91
M160H0.6 W (Wick debound)	61.38	37.96	0.52	1.62	99.87
M190H0.6	59.77	39.76	0.30	1.50	99.83
M190H0.6 W (Wick debound)	59.54	39.93	0.42	1.49	99.89
M190H20	59.60	39.69	0.57	1.50	99.86

* XX is the mixing temperature in °C.
** YY is the heating rate for the thermal debinding.

O-Si network bonds, resulting in the observed Al_2O_3/SiO_2 ratio of 1.5. When mixing at 160 °C and heat treating with a rate of 0.6 K/min, the release of unstable POSS molecules occurs before crosslinking takes place which reduces the yield of SiO_2. Even if a wick debinding step at 210 °C is implemented, the evaporation of volatile POSS molecules cannot be prevented, as a high fraction of molecules are already gradually eliminated below 210 °C. Based on these findings, it can be concluded that crosslinking of the preceramic polymer during the mixing step is a successful strategy to preserve a higher SiO_2 yield for thermoplastic processing like MEX-AM, even at slow heating rates.

Additionally, samples M160H0.6 and M190H0.6 were analyzed by XRD. As can be seen in Fig. 7a,b, conversion to mullite phase has been achieved. Also, an amorphous content between 2θ of 15° and 30° is visible. Successful dispersion of highly active alumina particles within the PCP matrix led to the prevention of cristobalite impurity. Similar behavior has been reported by other researchers [55,56]. However, using XRD analysis, no difference in the amorphous content could be detected between the two samples after sintering at 1700 °C for 5 h (Fig. 7c).

SEM and EDS element analysis were performed on the polished cross-

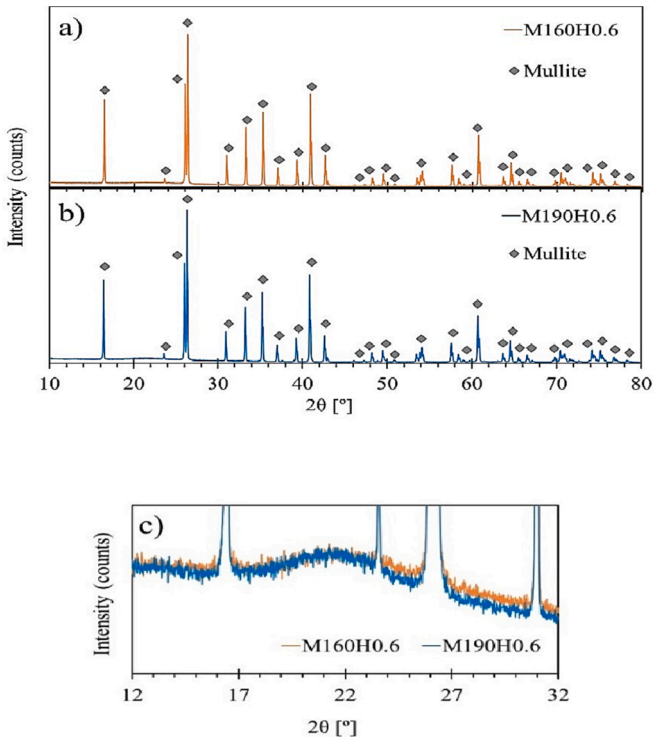

Fig. 7. XRD result of sintered mullite, mixed at a) 160 °C and b) 190 °C with a heating rate of 0.6 K/min, c) amorphous phase in both samples.

section of the sintered M190H0.6 sample as shown in Fig. 8a. The microstructure consisted of needle-like mullite grains with an amorphous phase in between. Element analysis was performed in the crystalline and amorphous area of the M190H0.6 sample (Fig. 8b), indicated as point 1 and point 2, respectively. As can be seen in Fig. 8c, both the crystalline and amorphous phases consisted of silicon (Si), aluminum (Al), oxygen (O), magnesium (Mg). Detected carbon (C) is associated with the carbon coating from the sputtering element. The presence of Mg element in the crystalline phase arises from the generated liquid phase by MgO between mullite grains in a narrow temperature range (1410–1425 °C) to promote densification, as reported by several studies [22,57–59]. The composition of the needle-like mullite crystals in point 1 refers to an alumina-rich aluminosilicate phase. Growth of elongated mullite grains has been reported by other studies as well [60]. Such anisotropic grain growth has been observed in mullite compositions, which contain less than 72 wt% Al_2O_3. When the sintering temperature is near or above the eutectic temperature (approximately 1590 °C), this microstructure appears due to the presence of the liquid phase [57,60]. The liquid phase facilitates the diffusion of atoms to promote the sintering process. It also plays an important role in the mass redistribution required for the microstructural transformation to elongated grains. Anisotropic grain growth is favorable as it reduces the grain boundary area and subsequently, the free energy of the system. The Al/Si ratio changes significantly between the crystalline and amorphous phases. Based on EDS analysis of point 2, we assume that MgO additive is partially dissolved in the amorphous phase and formed a silica-rich amorphous phase in Al_2O_3-SiO_2-MgO ternary system as it contains Al and Mg elements, as well. We assume that the glass phase and formed an MgO containing silica-rich ternary phase (MgO–Al_2O_3–SiO_2). A small amount of Na is due to contamination by touching the sample without gloves.

For comparison, the polished M160H0.6 sample was investigated by SEM and EDS analysis, as presented in Fig. 9. Based on Fig. 9c, an EDS analysis of point 1 depicts a distribution of Si, Al and O whereas an EDS analysis from point 2, represented Si, Al, O and Mg elements. It can be concluded that sample M160H0.6 contains an alumina-rich aluminosilicate crystalline phase, which is surrounded, by a silica-rich amorphous phase in Al_2O_3-SiO_2-MgO ternary system. MgO phase in sintered M160H0.6 sample is exclusively present in the SiO_2-rich amorphous phase.

4. Conclusions

In this study, the thermal behavior of a commercial methylsilsesquioxane (SILRES MK) was studied up to 800 °C under air and inert atmospheres. Based on TG analysis of pure MK resin, the heating

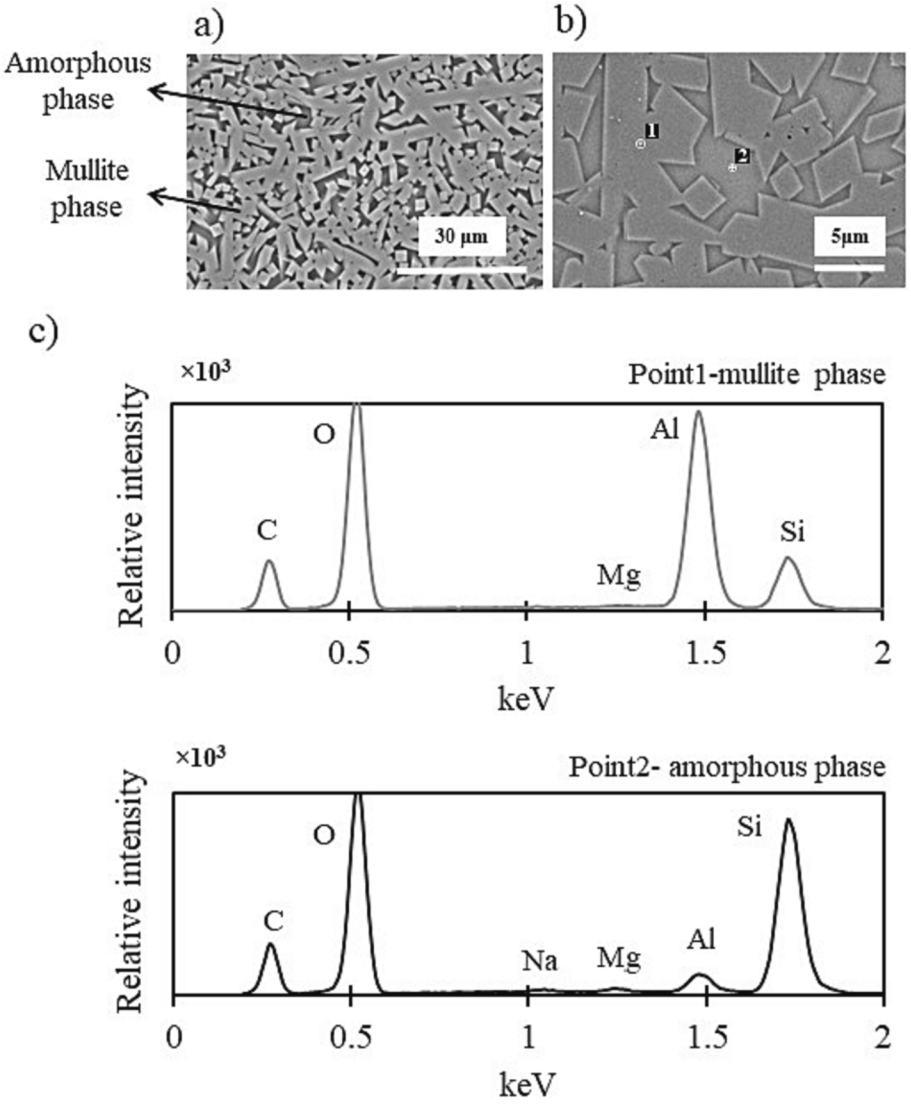

Fig. 8. a,b) microstructure of sintered m190h0.6 sample, c) eds elemental analysis of amorphous and mullite phase in (b) indicated as point 1 and 2, respectively.

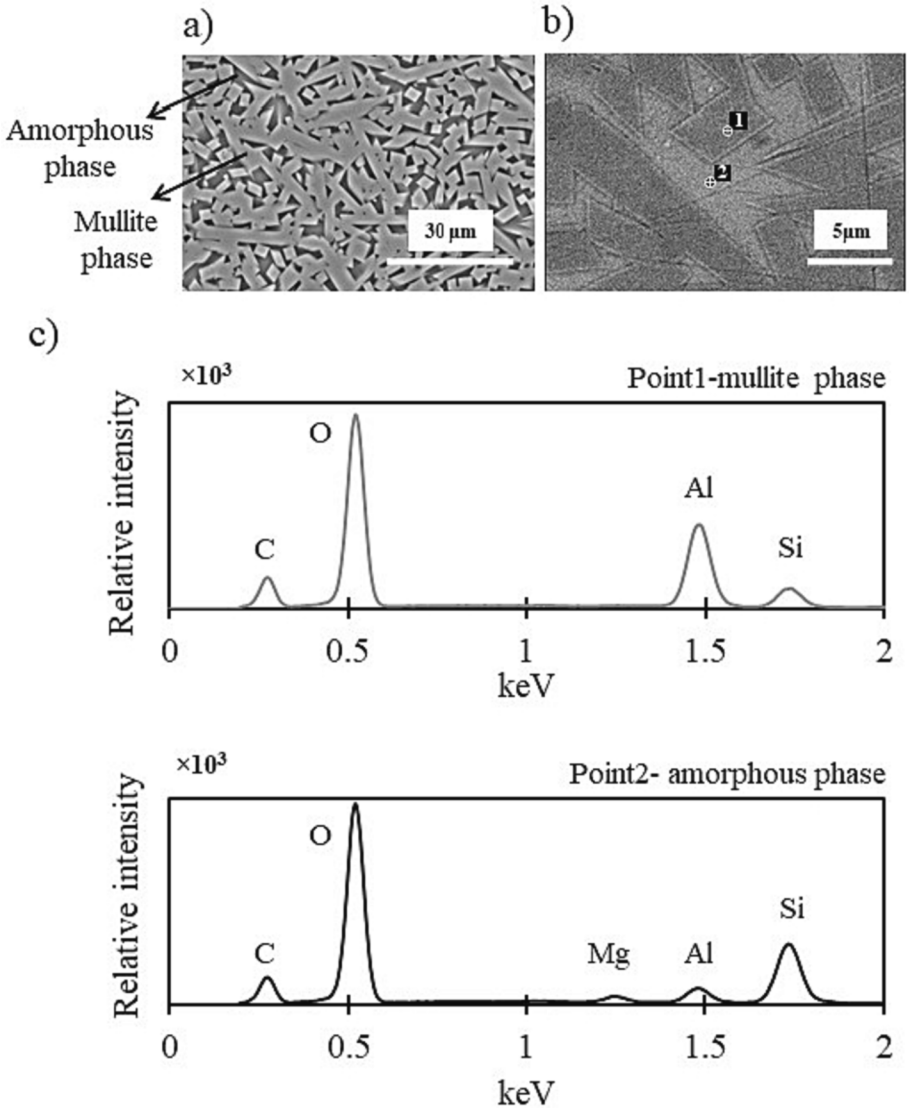

Fig. 9. a,b) microstructure of sintered m160h0.6 sample, c) eds elemental analysis of amorphous and mullite phase in (b) indicated as point 1 and 2, respectively.

rate is a crucial factor in determining the SiO_2 yield of the preceramic polymer after pyrolysis under air atmosphere. Heating slowly (below 2 K/min) in air reduces the SiO_2 yield as volatile species have a longer time to evaporate below the crosslinking temperature and a higher fraction of POSS molecules with cage structures will escape the structure. In thermoplastic processes like MEX-AM, low heating rates and dwell times are mandatory to remove binder without cracks, blisters and bobbles. Therefore, the instability of POSS molecules will significantly affect the fabrication of polymer derived oxide ceramics (e.g. silicate ceramics) with a defined silicon oxide content.

Mixing thermoplastic feedstocks at 160 °C (below the crosslinking temperature of MK) resulted in a SiO_2 deficiency during thermal debinding with a slow heating rate of 0.6 K/min. Interestingly, mixing the feedstock at 190 °C (above the crosslinking temperature of MK) with the same heating rate, provided a constant yield of 81 wt% and uncontrolled evaporation of POSS species could be avoided. This approach can be used for the fabrication of different polymer derived silicate ceramics with precise stoichiometric compositions using various thermoplastic shaping techniques such as pressing, extrusion, injection molding, and MEX-AM.

Scanning electron microscope images of sintered samples, mixed at 160 and 190 °C which were debound and pyrolyzed with a heating rate of 0.6 K/min resulted in the formation of needle-like mullite grains surrounded by an amorphous phase. Despite mixed sample at 190 °C, MgO was detected only in amorphous phase when mixing at 160 °C by EDS analysis. In the sample mixed at 190 °C, a low fraction of MgO has contributed to densification of the mullite phase as a sintering additive and the rest is mixed with the aluminosilicate amorphous phase. When mixing the sample at 160 °C, however, MgO is only visible in amorphous content.

CRediT authorship contribution statement

Fateme Sarraf: Conceptualization, Investigation, Methodology, Validation, Visualization, Writing – original draft, Review & editing. **Amir Hadian:** Methodology, Investigation, Writing – review & editing. **Frank Gfeller:** Methodology, Investigation. **Sergey V. Churakov:** Supervision, Writing – review & editing. **Frank Clemens:** Conceptualization, Funding acquisition, Methodology, Project administration, Supervision, Writing – review & editing.

Declaration of competing interest

The authors declare the following financial interests/personal relationships which may be considered as potential competing interests: Dr. Frank Clemens reports financial support was provided by Swiss

National Science Foundation..

Data availability

Data will be made available on request.

Acknowledgments

This work was supported by the Swiss National Science Foundation (SNSF) [grant number 200021_184691/1]. Authors would like to thank Beatrice Fischer and Robin Pauer for their help with the FT-IR and SEM measurements, respectively.

Appendix A. Supplementary data

Supplementary data to this article can be found online at https://doi.org/10.1016/j.matdes.2023.112578.

References

[1] F. Ainger, J. Herbert, The preparation of phosphorus-nitrogen compounds as non-porous solids, Special Ceramics 168 (1960) 81.
[2] S. Yajima, K. Okamura, J. Hayashi, Structural analysis in continuous silicon carbide fiber of high tensile strength, Chem. Lett. 4 (12) (1975) 1209–1212, https://doi.org/10.1246/cl.1975.1209.
[3] R.M. Laine, F. Babonneau, Preceramic polymer routes to silicon carbide, Chem. Mater. 5 (3) (1993) 260–279.
[4] G.T. Burns, G. Chandra, Pyrolysis of preceramic polymers in ammonia: preparation of silicon nitride powders, J. Am. Ceram. Soc. 72 (2) (1989) 333–337, https://doi.org/10.1111/j.1151-2916.1989.tb06129.x.
[5] G. Feiertag, W. Ehrfeld, H. Freimuth, H. Kolle, H. Lehr, M. Schmidt, M. Sigalas, C. Soukoulis, G. Kiriakidis, T. Pedersen, Fabrication of photonic crystals by deep x-ray lithography, Appl. Phys. Lett. 71 (11) (1997) 1441–1443, https://doi.org/10.1063/1.120431.
[6] P. Colombo, M. Modesti, Silicon oxycarbide ceramic foams from a preceramic polymer, J. Am. Ceram. Soc. 82 (3) (1999) 573–578, https://doi.org/10.1111/j.1151-2916.1999.tb01803.x.
[7] N.C. Fontão, M. Wilhelm, K. Rezwan, Asymmetric polysiloxane-based SiOC membranes produced via phase inversion tape casting process, Materials & Design 198 (109328) (2021), https://doi.org/10.1016/j.matdes.2020.109328.
[8] Q. Hanniet, E. Petit, S. Calas-Etienne, P. Etienne, K. Aissou, C. Gervais, P. Miele, B. Charlot, C. Salameh, Rational design of SiBCN microstructures using direct photolithography of patternable preceramic photoresists, Materials & Design 223 (111234) (2022), https://doi.org/10.1016/j.matdes.2022.111234.
[9] Y.W. Kim, H.D. Kim, C.B. Park, Processing of microcellular mullite, J. Am. Ceram. Soc. 88 (12) (2005) 3311–3315, https://doi.org/10.1111/j.1551-2916.2005.00597.x.
[10] E. Bernardo, E. Tomasella, P. Colombo, Development of multiphase bioceramics from a filler-containing preceramic polymer, Ceram. Int. 35 (4) (2009) 1415–1421, https://doi.org/10.1016/j.ceramint.2008.07.003.
[11] G. Parcianello, E. Bernardo, P. Colombo, Low temperature synthesis of zircon from silicone resins and oxide nano-sized particles, J. Eur. Ceram. Soc. 32 (11) (2012) 2819–2824, https://doi.org/10.1016/j.jeurceramsoc.2011.11.028.
[12] I.-H. Song, M.-J. Kim, H.-D. Kim, Y.-W. Kim, Processing of microcellular cordierite ceramics from a preceramic polymer, Scr. Mater. 54 (8) (2006) 1521–1525, https://doi.org/10.1016/j.scriptamat.2005.12.039.
[13] E. Bernardo, P. Colombo, S. Hampshire, SiAlON-based ceramics from filled preceramic polymers, J. Am. Ceram. Soc. 89 (12) (2006) 3839–3842, https://doi.org/10.1111/j.1551-2916.2006.01287.x.
[14] E. Bernardo, L. Fiocco, G. Parcianello, E. Storti, P. Colombo, Advanced Ceramics from Preceramic Polymers Modified at the Nano-Scale: A Review, Materials (2014) 1927–1956, https://doi.org/10.3390/ma7031927.
[15] Y.D. Blum, R.M. Platz, E.J. Crawford, Glass Strengthening by Polymer-Derived Ceramic Coatings, J. Am. Ceram. Soc. 73 (1) (1990) 170–172, https://doi.org/10.1111/j.1151-2916.1990.tb05116.x.
[16] J.D. Torrey, R.K. Bordia, Processing of polymer-derived ceramic composite coatings on steel, J. Am. Ceram. Soc. 91 (1) (2008) 41–45, https://doi.org/10.1111/j.1551-2916.2007.02019.x.
[17] C.H. Park, Y.J. Joo, J.K. Chung, Y.H. Han, C.J. Kim, Morphology control of a silicon nitride thick film derived from polysilazane precursor using UV curing and IR heat treatment, Adv. Appl. Ceram. 116 (7) (2017) 376–382, https://doi.org/10.1080/17436753.2017.1339490.
[18] L. Gorjan, R. Tonello, T. Sebastian, P. Colombo, F. Clemens, Fused deposition modeling of mullite structures from a preceramic polymer and γ-alumina, J. Eur. Ceram. Soc. 39 (7) (2019) 2463–2471, https://doi.org/10.1016/j.jeurceramsoc.2019.02.032.
[19] T. Takahashi, H. Münstedt, M. Modesti, P. Colombo, Oxidation resistant ceramic foam from a silicone preceramic polymer/polyurethane blend, J. Eur. Ceram. Soc. 21 (16) (2001) 2821–2828, https://doi.org/10.1016/S0955-2219(01)00220-5.
[20] J. Zeschky, T. Höfner, C. Arnold, R. Weißmann, D. Bahloul-Hourlier, M. Scheffler, P. Greil, Polysilsesquioxane derived ceramic foams with gradient porosity, Acta Mater. 53 (4) (2005) 927–937, https://doi.org/10.1016/j.actamat.2004.10.039.
[21] C. Vakifahmetoglu, D. Zeydanli, P. Colombo, Porous polymer derived ceramics, Mater. Sci. Eng. R. Rep. 106 (2016) 1–30, https://doi.org/10.1016/j.mser.2016.05.001.
[22] F. Sarraf, E. Abbatinali, L. Gorjan, T. Sebastian, P. Colombo, S.V. Churakov, F. Clemens, Effect of MgO sintering additive on mullite structures manufactured by fused deposition modeling (FDM) technology, J. Eur. Ceram. Soc. 41 (13) (2021) 6677–6686, https://doi.org/10.1016/j.jeurceramsoc.2021.06.012.
[23] P. Greil, Active-filler-controlled pyrolysis of preceramic polymers, J. Am. Ceram. Soc. 78 (4) (1995) 835–848, https://doi.org/10.1111/j.1151-2916.1995.tb08404.x.
[24] F. Sarraf, A. Hadian, S.V. Churakov, F. Clemens, EVA-PVA binder system for polymer derived mullite made by material extrusion based additive manufacturing, J. Eur. Ceram. Soc. 43 (2) (2023) 530–541, https://doi.org/10.1016/j.jeurceramsoc.2022.10.009.
[25] P. Colombo, G. Mera, R. Riedel, G.D. Sorarù, Polymer-Derived Ceramics: 40 Years of Research and Innovation in Advanced Ceramics, J. Am. Ceram. Soc. (2010), https://doi.org/10.1111/j.1551-2916.2010.03876.x.
[26] E. Rosado, R. Moreno, Mullite-silica scaffolds obtained by stereolithography and reaction sintering, Open Ceramics 14 (2023), 100361, https://doi.org/10.1016/j.oceram.2023.100361.
[27] J. Essmeister, A.A. Altun, M. Staudacher, T. Lube, M. Schwentenwein, T. Konegger, Stereolithography-based additive manufacturing of polymer-derived SiOC/SiC ceramic composites, J. Eur. Ceram. Soc. 42 (13) (2022) 5343–5354, https://doi.org/10.1016/j.jeurceramsoc.2022.06.021.
[28] M. Wang, C. Xie, R. He, G. Ding, K. Zhang, G. Wang, D. Fang, Polymer-derived silicon nitride ceramics by digital light processing based additive manufacturing, J. Am. Ceram. Soc. 102 (9) (2019) 5117–5126, https://doi.org/10.1111/jace.16389.
[29] J. Schmidt, A.A. Altun, M. Schwentenwein, P. Colombo, Complex mullite structures fabricated via digital light processing of a preceramic polysiloxane with active alumina fillers, J. Eur. Ceram. Soc. 39 (4) (2019) 1336–1343, https://doi.org/10.1016/j.jeurceramsoc.2018.11.038.
[30] M. Pelanconi, P. Colombo, A. Ortona, Additive manufacturing of silicon carbide by selective laser sintering of PA12 powders and polymer infiltration and pyrolysis, J. Eur. Ceram. Soc. 41 (10) (2021) 5056–5065, https://doi.org/10.1016/j.jeurceramsoc.2021.04.014.
[31] N. Kamboj, M. Aghayan, C.S. Rodrigo-Vazquez, M.A. Rodríguez, I. Hussainova, Novel silicon-wollastonite based scaffolds for bone tissue engineering produced by selective laser melting, Ceram. Int. 45 (18) (2019) 24691–24701, https://doi.org/10.1016/j.ceramint.2019.08.208.
[32] J.W. Kemp, A.A. Diaz, E.C. Malek, B.P. Croom, Z.D. Apostolov, S.R. Kalidindi, B. G. Compton, L.M. Rueschhoff, Direct ink writing of ZrB2-SiC chopped fiber ceramic composites, Addit. Manuf. 44 (2021), 102049, https://doi.org/10.1016/j.addma.2021.102049.
[33] K. Huang, H. Elsayed, G. Franchin, P. Colombo, Embedded direct ink writing of freeform ceramic components, Appl. Mater. Today 23 (2021), 101005, https://doi.org/10.1016/j.apmt.2021.101005.
[34] L. Zhao, X. Wang, H. Xiong, K. Zhou, D. Zhang, Optimized preceramic polymer for 3D structured ceramics via fused deposition modeling, J. Eur. Ceram. Soc. 41 (10) (2021) 5066–5074, https://doi.org/10.1016/j.jeurceramsoc.2021.03.061.
[35] G. El Chawich, J. El Hayek, V. Rouessac, D. Cot, B. Rebière, R. Habchi, H. Garay, M. Bechelany, M. Zakhour, P. Miele, C. Salameh, Design and Manufacturing of Si-Based Non-Oxide Cellular Ceramic Structures through Indirect 3D Printing, Materials (2022), https://doi.org/10.3390/ma15020471.
[36] A. Kulkarni, G.D. Sorarù, J.M. Pearce, Polymer-derived SiOC replica of material extrusion-based 3-D printed plastics, Addit. Manuf. 32 (2020), 100988, https://doi.org/10.1016/j.addma.2019.100988.
[37] H. Mei, Y. Yan, L. Feng, K.G. Dassios, H. Zhang, L. Cheng, First printing of continuous fibers into ceramics, J. Am. Ceram. Soc. 102 (6) (2019) 3244–3255, https://doi.org/10.1111/jace.16234.
[38] A. Kulkarni, J. Pearce, Y. Yang, A. Motta, G.D. Sorarù, SiOC (N) cellular structures with dense struts by integrating fused filament fabrication 3D printing with polymer-derived ceramics, Adv. Eng. Mater. 23 (12) (2021) 2100535, https://doi.org/10.1002/adem.202100535.
[39] H. Tian, Q.-S. Ma, Effects of heating rate on the structure and properties of SiOC ceramic foams derived from silicone resin, Ceram. Int. 38 (3) (2012) 2101–2104, https://doi.org/10.1016/j.ceramint.2011.10.048.
[40] E. Bernardo, P. Colombo, E. Pippel, J. Woltersdorf, Novel mullite synthesis based on alumina nanoparticles and a preceramic polymer, J. Am. Ceram. Soc. 89 (5) (2006) 1577–1583, https://doi.org/10.1111/j.1551-2916.2006.00963.x.
[41] F. Clemens, A. Kerber, FDM/FFF an Alternative to CIM Manufacturing of Prototype and Small Quantities of Ceramic Part, Ceram Appl 8 (27–31) (2020).
[42] A. Nazir, O. Gokcekaya, K. Billah, O. Ertugrul, J. Jiang, J. Sun, S. Hussain, Multi-material additive manufacturing: A systematic review of design, properties, applications, challenges, and 3D Printing of materials and cellular metamaterials, Mater. Des. 111661 (2023), https://doi.org/10.1016/j.matdes.2023.111661.
[43] E. Bernardo, P. Colombo, E. Dainese, G. Lucchetta, P.F. Bariani, Novel 3D wollastonite-based scaffolds from preceramic polymers containing micro-and nano-sized reactive particles, Adv. Eng. Mater. 14 (4) (2012) 269–274, https://doi.org/10.1002/adem.201100241.
[44] G. Parcianello, E. Bernardo, P. Colombo, Cordierite ceramics from silicone resins containing nano-sized oxide particle fillers, Ceram. Int. 39 (8) (2013) 8893–8899, https://doi.org/10.1016/j.ceramint.2013.04.083.

[45] R. Harshe, C. Balan, R. Riedel, Amorphous Si(Al)OC ceramic from polysiloxanes: bulk ceramic processing, crystallization behavior and applications, J. Eur. Ceram. Soc. 24 (12) (2004) 3471–3482, https://doi.org/10.1016/j.jeurceramsoc.2003.10.016.
[46] J. Ma, F. Ye, S. Lin, B. Zhang, H. Yang, J. Ding, C. Yang, Q. Liu, Large size and low density SiOC aerogel monolith prepared from triethoxyvinylsilane/tetraethoxysilane, Ceram. Int. 43 (7) (2017) 5774–5780, https://doi.org/10.1016/j.ceramint.2017.01.124.
[47] S. Tsuge, H. Ohtani, C. Watanabe, Pyrolysis-GC/MS data book of synthetic polymers: pyrograms, thermograms and MS of pyrolyzates, Elsevier, 2011.
[48] E. Ionescu, C. Linck, C. Fasel, M. Müller, H.J. Kleebe, R. Riedel, Polymer-derived SiOC/ZrO2 ceramic nanocomposites with excellent high-temperature stability, J. Am. Ceram. Soc. 93 (1) (2010) 241–250, https://doi.org/10.1111/j.1551-2916.2009.03395.x.
[49] F. Vivier, D. Santamaria, D. Pellerej, P. Buonfico, M. Sangermano, A kinetic analysis of a thermal curing reaction of a silicon resin in solid state, Characterization of Minerals, Metals, and Materials 2014 (2014) 63–72.
[50] K. Kanamori, Monolithic silsesquioxane materials with well-defined pore structure, J. Mater. Res. 29 (23) (2014) 2773–2786.
[51] K. Papakollu, N. Moharana, K.H. Kumar, S. Lauterbach, H.-J. Kleebe, E. Ionescu, R. Kumar, Synthesis and temperature-dependent evolution of the phase composition in palladium-containing silicon oxycarbide ceramics, J. Eur. Ceram. Soc. 42 (12) (2022) 4825–4834, https://doi.org/10.1016/j.jeurceramsoc.2022.05.032.
[52] W.-C. Liu, C.-C. Yang, W.-C. Chen, B.-T. Dai, M.-S. Tsai, The structural transformation and properties of spin-on poly (silsesquioxane) films by thermal curing, J. Non Cryst. Solids 311 (3) (2002) 233–240, https://doi.org/10.1016/S0022-3093(02)01373-X.
[53] E. Radovanovic, M. Gozzi, M. Gonçalves, I. Yoshida, Silicon oxycarbide glasses from silicone networks, J. Non Cryst. Solids 248 (1) (1999) 37–48, https://doi.org/10.1016/S0022-3093(99)00101-5.
[54] A. Tamayo, R. Peña-Alonso, F. Rubio, J. Rubio, J. Oteo, Synthesis and characterization of boron silicon oxycarbide glass fibers, J. Non Cryst. Solids 358 (2) (2012) 155–162, https://doi.org/10.1016/j.jnoncrysol.2011.09.002.
[55] D. Suttor, H.J. Kleebe, G. Ziegler, Formation of mullite from filled siloxanes, J. Am. Ceram. Soc. 80 (10) (1997) 2541–2548, https://doi.org/10.1111/j.1151-2916.1997.tb03156.x.
[56] E. Bernardo, P. Colombo, E. Manias, SiOC glass modified by montmorillonite clay, Ceram. Int. 32 (6) (2006) 679–686, https://doi.org/10.1016/j.ceramint.2005.05.002.
[57] Y. Dong, S. Hampshire, J.-E. Zhou, Z. Ji, J. Wang, G. Meng, Sintering and characterization of flyash-based mullite with MgO addition, J. Eur. Ceram. Soc. 31 (5) (2011) 687–695, https://doi.org/10.1016/j.jeurceramsoc.2010.12.012.
[58] L. Montanaro, C. Perrot, C. Esnouf, G. Thollet, G. Fantozzi, A. Negro, Sintering of industrial mullites in the presence of magnesia as a sintering aid, J. Am. Ceram. Soc. 83 (1) (2000) 189–196, https://doi.org/10.1111/j.1151-2916.2000.tb01169.x.
[59] R.G. Chandran, B. Chandrashekar, C. Ganguly, K. Patil, Sintering and microstructural investigations on combustion processed mullite, J. Eur. Ceram. Soc. 16 (8) (1996) 843–849, https://doi.org/10.1016/0955-2219(96)00001-5.
[60] T. Huang, M.N. Rahaman, T.I. Mah, T.A. Parthasarathay, Anisotropic grain growth and microstructural evolution of dense mullite above 1550 C, J. Am. Ceram. Soc. 83 (1) (2000) 204–210, https://doi.org/10.1111/j.1151-2916.2000.tb01171.x.